PERGAMON

Chemical Engineering Science 56 (2001) 2715–2720

Chemical Engineering Science

www.elsevier.nl/locate/ces

Time-dependent finite-volume simulation of the turbulent flow in a free-surface CSTR

Alessandro Serra, Marina Campolo, Alfredo Soldati*

Centro Interdipartimentale di Fluidodinamica e Idraulica, and Dipartimento di Scienze e Tecnologie Chimiche, Università degli Studi di Udine, 1-33100 Udine, Italy

Received 21 April 2000; received in revised form 6 October 2000; accepted 9 October 2000

Abstract

Finite-volume numerical simulations of the flow field in a curved-bottom, free-surface reactor are presented. Full transient simulations with explicit modeling of the air–water interface are made in order to reproduce correctly the entire flow field in the vessel. Qualitative comparison of numerical results is given against literature and experimental data. We discuss critically the measurements of the extent of transient duration for the different simulations, and of the axial flowrate. Furthermore, we try to evaluate the importance of the free-surface deformation. In order to evaluate this, we calculate the energy required to shape the free surface, which we find to be up to 6% of the fluid kinetic energy. Finally, we evaluate the stirring capability of the reactor in different working conditions.

Keywords: Chemical reactors; Dynamic simulation; Interface; Numerical analysis; CFD

1. Introduction

Continuously stirred tank reactors (CSTR) are used to enhance mixing of reacting species in a number of industrial processes. Industrial CSTRs are cylindrical tanks with curved bottom equipped with single or multiple impellers. In order to obtain optimal reaction rates and, consequently, optimal operating costs, geometry of the vessel and of the impeller, as well as impeller off-bottom clearance and revolutions per minute (RPM) must be optimized (Tatterson, Brodkey, & Calabrese, 1991; Zhou & Kresta, 1996). Current design optimization, based on semi-empirical approaches, is not fully satisfactory. Experimental techniques used to investigate flow fields, heat fluxes, and mass concentration fields in CSTRs are extremely costly (Tatterson, Yuan, & Brodkey, 1980; Ranade, Joshi, & Marathe, 1989; Fort, Vonzy, & Forstova, 1991; Jaworski, Nienow, Koutsakos, Dyster, & Bujalski, 1991; Ranade, Bourne, & Joshi, 1991; Kresta & Wood, 1993a; Armenante & Chou, 1996; Hockey & Nouri, 1996; Schafer, Yianneskis, Wachter, & Durst, 1998) and may not be applied to many configurations for industrial mixers. In addition, results obtained for laboratory vessels are not, in general, scalable to industrial size plants, especially with multiphase flows. Full numerical analyses of the flow field are difficult, given the complexity of momentum balance equation for the fluid. Only recently, developments of numerical solvers — and of computers — allowed to calculate the three-dimensional time-dependent flow field in complex geometries. Numerical simulations of CSTRs have to face the following two main geometrical complexities: first, the relative position of the baffled vessel and the rotating impeller changes continuously through time; second, the presence of the free interface between the liquid and the above atmosphere requires specific treatment. In the literature, most of numerical analysis of the flow field in CSTRs were performed under the following simplificative assumptions: (i) simple geometry for impeller and vessel — i.e. flat bottom and closed flat top (Kresta & Wood, 1993a, b; Sahu & Joshi, 1995; Armenante & Chou, 1996; Sahu, Kumar, & Joshi, 1998; Brucato, Ciofalo, Grisafi, & Micale, 1998; Sahu, Kumar, Patwardhan, & Joshi, 1999; Wechsler, Breuer, & Durst, 1999); (ii) steady state — i.e. the effect of blades is averaged over the impeller revolution period (Harvey, Lee, & Rogers, 1995; Wechsler et al., 1999); and (iii) closed surface or flat free surface

* Corresponding author. Tel.: + 39-0-432-558864; fax: + 39-0-432-558803.

E-mail address: alfredo@euterpe.dstc.uniud.it (A. Soldati).

0009-2509/01/$ - see front matter
PII: S0009-2509(00)00519-4

— i.e. axial symmetry plane boundary condition at the vessel top (Harvey et al., 1995; Brucato et al., 1998). This is due to the need of a systematic approach to gain physical insights. Yet, possibly due to these simplificative assumptions, inaccuracies in the flow field led to overestimate the axial velocity near the interface (Harvey et al., 1995), and to miscalculate the energy balance. Recently, Ciofalo, Brucato, Grisafi, and Torraca (1996) examined the free-surface deformation and its effect on the flow field for an unbaffled tank. In this work, we couple the investigation of the free-surface deformation in a baffled tank together with full transient analysis of the flow field. The examined CSTR is characterized by a curved bottom, and the starting condition for the simulations is still fluid. A complex geometry, a full-transient simulation and the explicit development of the wavy surface are considered together to demonstrate that simplifying assumptions required in the past to overcome the lack of computational resources can be relaxed and detailed simulations of industrial mixers can be made. Objectives of this work are, first, to identify the extent of the start-up phase, during which time dependence of the flow field may not be neglected; second, to quantify the stirring capability of the impeller, measured by the circulation induced in the vessel; third, to identify the behavior of the free surface and its effect on the energy balance; and fourth, to evaluate the stirring in the reactor.

We reproduced the behavior of a three-phase experimental reactor which will be fully operative soon (Bertolaccini, 1998). Vessel and impeller geometry is shown in Fig. 1, with dimensions reported in Table 1. In the final experimental configuration, the solid suspension and bubbles will interact in the reactor. Bubbles, blown at the bottom of the vessel, are distributed in the cross section by the sparger of the impeller, which also holds the six blades tilted by 45°. The four baffles are used to induce axial flows at the walls and enhance solid suspension. Little experimental data is currently available, except for qualitative data on the shape of the air–water interface.

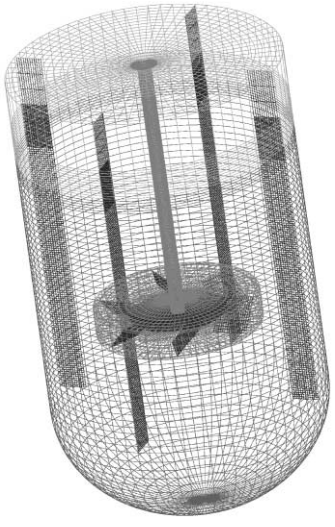

Fig. 1. Computational domain: air region, in light gray, outer region (static frame), and impeller and shaft region (rotating frame). Baffles and impeller are in dark gray.

Table 1
Geometric dimensions of vessel and impeller

Vessel diameter	$D = 0.20$ m
Impeller diameter	$d = 0.1$ m
Shaft diameter	$d_s = 0.012$ m
Baffle width	$B = 0.020$ m
Impeller clearance	$C = 0.065$ m
Impeller height	$H_i = 0.020$ m
Water height	$H_w = 0.20$ m
Vessel height	$H = 0.40$ m
Bottom depth	$H_b = 0.085$ m

2. Methodology

For the unsteady, incompressible fluid flow under consideration, the Reynolds averaged Navier–Stokes equations combined with a standard $k-\varepsilon$ turbulence model were solved using finite-volume discretization. The commercial package used is Star-CD. Present simulations are computationally intensive, given the time required to calculate the full transient. Furthermore, the analysis of the free surface requires the use of a two-fluid model to compute the distribution of the additional scalar, volume of fluid (VOF), used to identify the free-surface position. To reduce numerical diffusion for this scalar, a constraint on the time step is imposed. In order to reduce the overall computational effort, we decided to employ a $k-\varepsilon$ model to simulate turbulence. This model gives accurate results provided grid refinement close to the wall is accurate (Bartels, Breuer, & Durst, 2000). We chose a grid refinement in accordance to what was indicated by Bartels et al. (2000).

A tune-up procedure and a grid-independence analysis (Brucato et al., 1998; Sahu et al., 1998; Sahu et al., 1999) led to the computational domain shown in Fig. 1. The computational domain is divided into the following regions: (i) upper fluid, air, in light gray, bounded by the air–liquid interface and the vessel open top; (ii) shaft and impeller region, the part which moves during the simulation; external region, composed of a cylindrical body (iii) and a round bottom (iv). Baffles at the wall, in dark gray extend up to the top of the vessel. Boundary conditions are no-slip at the wall, no-slip at blades and shaft, and symmetry condition at the top of the air layer.

The discretization of the computational domain is summarized in Table 2. A uniform meshing was used, except in the near-wall region and in the region near the

Table 2
Discretization of computational domain

Air–water region	$r \times \theta \times z$	$20 \times 72 \times 20$
Impeller region	$r \times \theta \times z$	$12 \times 72 \times 4$
Cylindrical region out of the impeller	$r \times \theta \times z$	$20 \times 72 \times 40$
Curved bottom	$r \times \theta \times \phi$	$20 \times 72 \times 20$

air–water interface, where a finer mesh in the z-direction was required to track the interface accurately (Jeong & Yang, 1998). The dynamics of the interface was simulated based on a volume tracking technique. In the two fluid region, the volume fraction of water (VOF) — unity where there is only water, zero where there is only air — is used to identify the position of the interface for each computational cell. Values of VOF are updated in time by solving the transport equation. To reconstruct the time evolution of the free-surface profile from VOF data, a piecewise linear interface calculation (PLIC) technique was used (Issa & Ubbink, 1999; Scardovelli & Zaleski, 1999). The continuous free surface is approximated by a faceted plane, each facet spanning the region of a computational cell where VOF is strictly in the range 0–1. The facets delimit a volume equal to the local VOF in the cell and the facet normal is fixed from VOF value of neighboring cells to ensure continuity of the resulting faceted free surface.

To simulate the unsteady flow in the vessel, we used the sliding mesh approach in which the inner rotating mesh — i.e. part (ii) of the computational domain — is coupled to the steady outer mesh through a sliding interface allowing exchange of velocity and pressure information. The governing equations — i.e. mass, momentum, turbulent kinetic energy and rate of dissipation — are solved using a rotating frame of reference in the impeller region and a static frame of reference in the rest of the domain. The simulation started from condition of still fluid filling the tank up to a level H_w.

3. Results

The first object of the simulation was to examine the evolution of the flow structure until the pseudo-steady state was attained. Here, we consider the flow field to be pseudo-steady when time dependence is not associated to the development of the flow structure but only to the blade frequency. In the pseudo-steady state the statistics of flow variables and the free-surface deformation show a time dependence which is a straightforward function of the blade frequency. We ran our simulation until first-order moments — i.e. axial flowrates — did not show time dependence except for that of the blade frequency. We performed four different simulations at 70, 140, 210 and 280 RPM. In Fig. 2(a), the period-averaged value of the axial flowrates is shown for the different simulations versus the axial coordinate, z. The peak corresponds to the lower part of the blades — i.e. discharge flux. The time necessary to reach the pseudo-steady state at 70, 140, 210 and 280 RPM was 9.3, 4.4, 3.1 and 2.7 s, respectively, corresponding to 11, 11, 11 and 12 complete impeller revolutions. In Fig. 2(b), the evolution of the axial flowrate is shown for the case at 140 RPM. Since the blades pump downward, the mean flow structure appears to evolve more rapidly in the lower part of the tank rather than in the upper part, closer to the interface. The pseudo-steady flow field at the different RPM was used to compute the power number, N_P. Power input to the fluid was obtained from the torque required to rotate the turbine, integrating pressure and viscous forces over all the surfaces of the turbine, blades, shaft and impeller disk (Harvey & Rogers, 1996). We found that torque is essentially due to pressure forces and the power number at the different RPM examined, corresponding to Reynolds between 11,600 and 46,400,

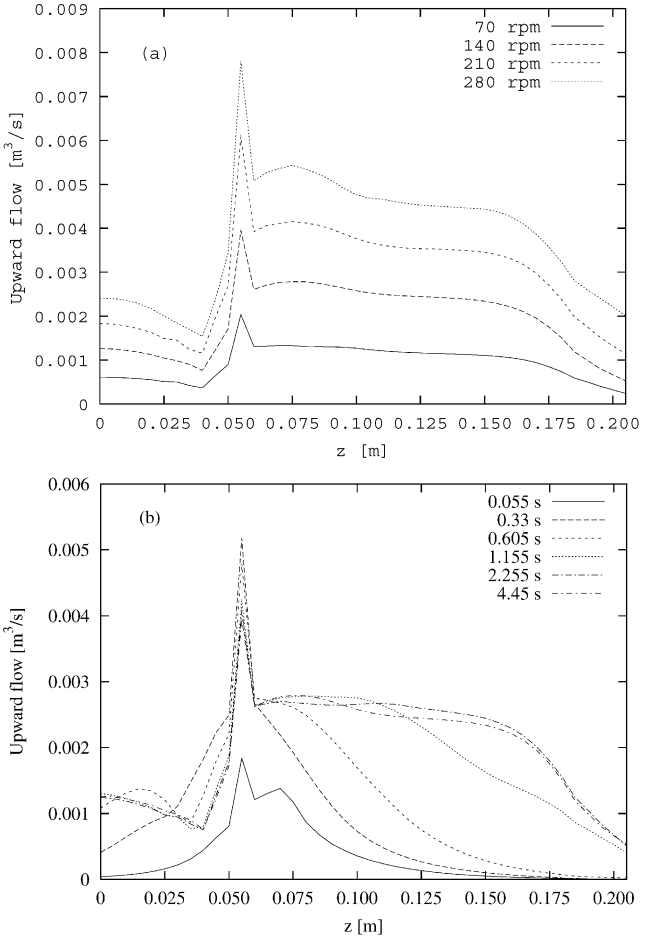

Fig. 2. Axial flow in vessel: (a) period-averaged pseudo-steady state values at 70, 140, 210 and 280 RPM; (b) evolution from initial condition of still fluid at 140 RPM.

was found to be in the range from 3.82 to 3.84. We are not aware of experimental work reported in the literature for a geometry similar to the one considered in this work, characterized by the curved bottom. Nevertheless, power number values in a wide range (from 0.87 to 4.8) are reported for downflow pitched blade impellers (Ranade & Joshi, 1989). Furthermore, empirical correlations provided by Nagata (1975) allow to derive a power number of 4.0 for the investigated configuration.

3.1. Air–water interface

At present, the status of the experimental facility (Bertolaccini, 1998) does not allow quantitative measurements. However, it is rather easy to measure the variation of the air–liquid interface at the wall with some accuracy. Since the shape of the free surface is controlled by the fluid dynamics of the entire flow field, we used the interface elevation to validate the accuracy of our calculations. As discussed before, from the behavior of the concentration of the volume fraction of water, calculated solving the transport equation for the scalar VOF through a high-order differencing scheme to avoid smearing of gradients, we reconstructed the interface profile for different sections by processing the VOF field through the PLIC method (Issa & Ubbink, 1999; Scardovelli & Zaleski, 1999). In Fig. 3, we show the comparison of the time-averaged computed interface at the wall against the qualitative experimental data. The trend seems captured correctly, even though at present we cannot justify discrepancies between our simulation and experimental data. In Fig. 3, we observe that the mean elevation of the free surface is larger as the rotation speed is increased, since centrifugal forces are larger. Also, the highest water level is found just upstream the baffles ($\theta = 0$ and 90°), where the fluid rises before bypassing the obstacle. Elevation of the free surface found at the wall of the vessel is balanced by depression of the fluid in the central region. In Fig. 4, the profile of the interface is shown for different radial sections. In proximity of the wall, the deviation from elevation at rest is larger for larger rotation speed, particularly for radial sections closer to baffles ($\theta = 0$ and 89°). This is balanced by larger depression of the interface near the shaft as the rotation speed is increased. As discussed by Harvey et al. (1995), a correct evaluation of the interface seems to be crucial for the accuracy of the flow field. From an overall energy balance it is evident that the energy supplied by

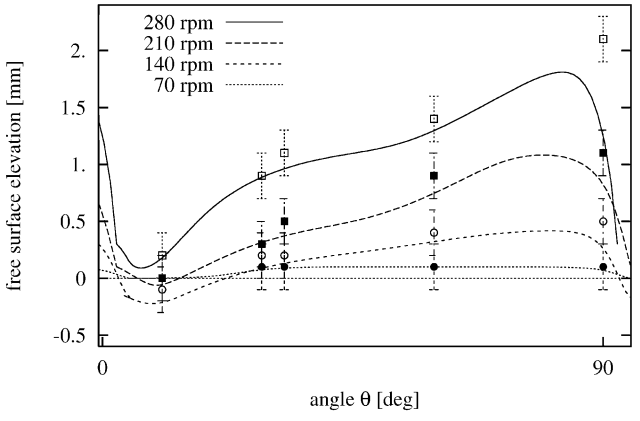

Fig. 3. Air–water profile at the wall: computed profile (lines) and qualitative experimental trend (symbols).

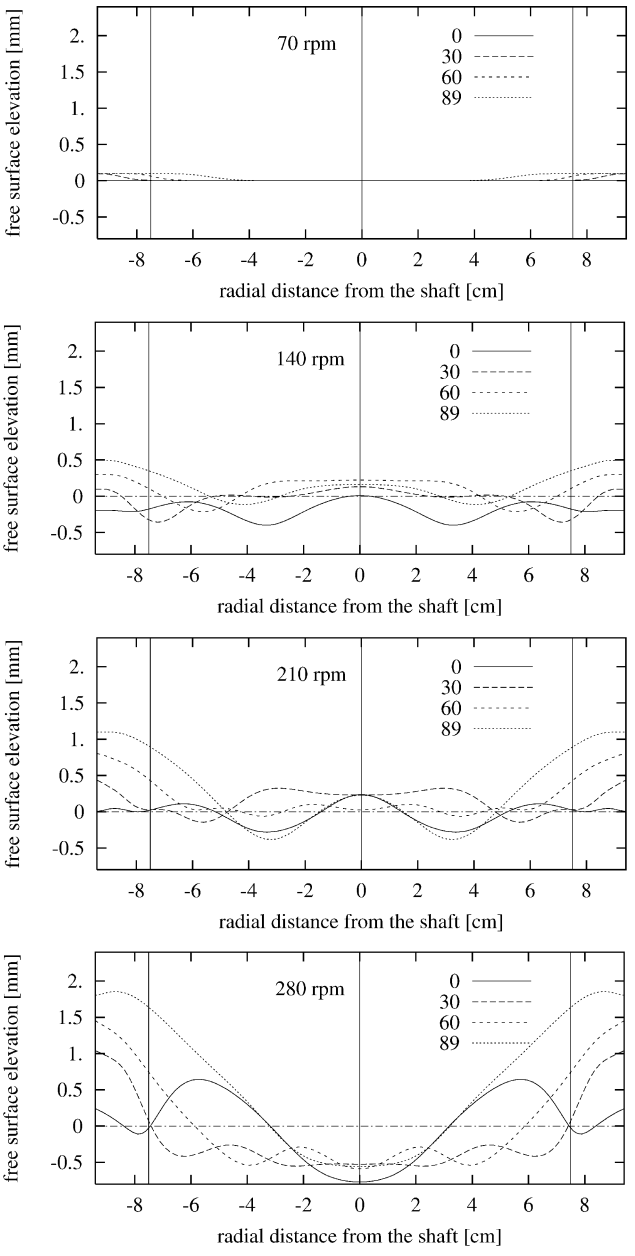

Fig. 4. Free-surface profile for different radial sections (0, 30, 60 and 89°) at 70, 140, 210 and 280 RPM.

the impeller is exploited to stir the flow field and to modify the interface. Neglecting the energy contribution required to shape the interface, which in turn impacts on both velocity profile and turbulence structure near the interface (De Angelis, 1998), may lead to inaccuracy in the overall computation. We calculated that a flat free-surface approximation would have increased the kinetic energy available for the fluid from 2.9% for the slower rotation speed up to 6% for the simulation at highest rotation speed.

A three-dimensional picture of the air–water interface when pseudo-stationary conditions have been obtained is shown in Fig. 5 for different rotation speeds (70, 140, 210 and 280 RPM from bottom to top). A complex wavy surface develops at the interface, and waves become larger as the rotation speed increases. For rotation speed equal to 70 RPM, the variation of the water surface is almost negligible. In the other cases, waves form upstream the baffles, generating peaks and throats of waves. In these regions, the fluid undergoes acceleration and air entrainment can occur. From Fig. 5, baffles appear, as expected, to be the main cause for the complex deformation dynamics of the water surface. However, the influence of the periodic motion of the blades is still perceptible at the free surface, even though the impeller is far below it. This is hardly visible in the snapshots shown here, but can be appreciated from time-sequence animations.

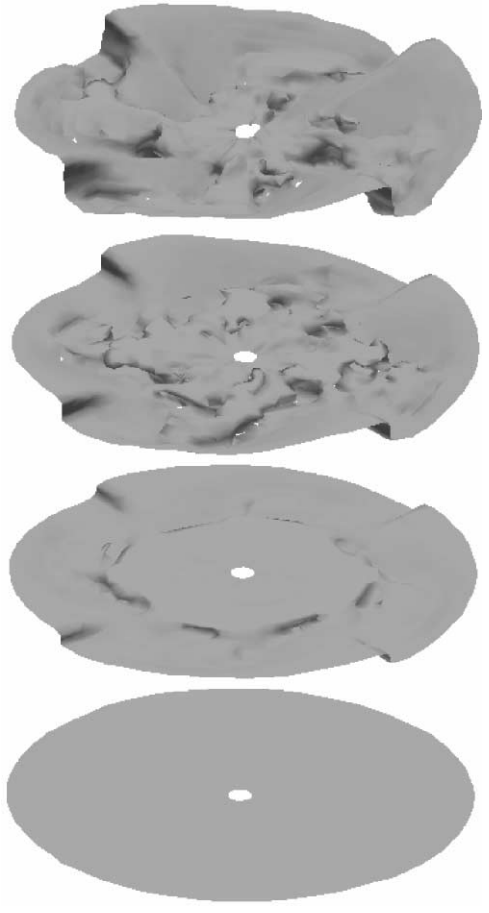

Fig. 5. Free surfaces at 70, 140, 210 and 280 RPM, from bottom to top.

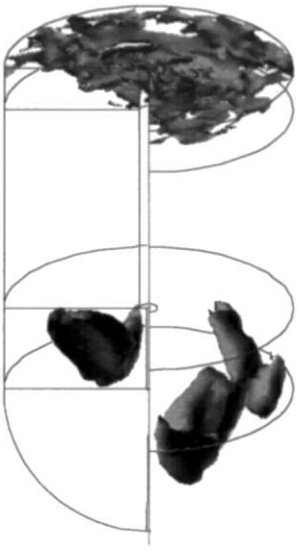

Fig. 6. Low-velocity regions at 210 RPM. Velocity isosurface is 5% of maximum value — blade tip velocity.

3.2. Macromixing

A complete knowledge of the complex flow field developing in the vessel is crucial to evaluate the stirring capability of the reactor. Steady, low-velocity regions identify regions of poor macromixing. Where macromixing is reduced, mixing relies only on micromixing which develops with longer time scales. Micromixing is also related to turbulence intensity and lower turbulence levels are frequently found in low-velocity regions. Flow field visualizations were made to identify low-velocity regions in the reactor under study. Since the magnitude of velocity vectors is strongly related to rotation speed, low-velocity regions must be identified with reference to each rotation speed. For each rotation speed, maximum of velocity was found at the blades where fluid is pumped downward in the radial direction. Impeller tip velocity was taken as the reference velocity for low-flow region identification. In Fig. 6, the regions where velocity modulus was less than 5% of the tip velocity are shown for the case at 210 RPM, over 270° degrees of the domain. Low-velocity regions are found in the curved bottom, slightly downstream the baffles, and in the proximity of the free surface. These regions are stationary and similar in shape for different rotation speeds. Whereas low-velocity regions at the bottom of the tank are likely to be destroyed by the gas bubbles, this may not be the case for the low-velocity, low-stirring regions next to the free surface (see also Fig. 2). It is apparent that the

identification of low-velocity regions may be of critical importance for industrial mixers.

4. Conclusions

In this work, we considered different pieces of information that can be obtained by numerical simulations of industrial mixers. We used a commercial CFD code to characterize the transient and pseudo-stationary behavior of a CSTR used to produce solid suspensions. The vessel, baffled, with an open top and a curved bottom, has a configuration similar to many reactors widely used for industrial applications. Numerical simulations of this configuration are scarce in literature, due to the computational effort required for modeling the round-bottom and the air–water interface. Simulations were performed for different rotation speeds starting from fluid at rest. Discussion about computational domain discretization, criteria for achievement of regime conditions and free-surface tracking was made in order to provide useful guidance for future implementation of CFD simulation of industrial vessels. Further numerical analysis for multiphase flow and quantitative comparison with experimental results are required to extend the validity of present results.

Acknowledgements

Financial support from MURST under Grant 9809326392_005 is gratefully acknowledged.

References

Armenante, P. M., & Chou, C. C. (1996). Velocity profiles in baffled vessel with single or double pitched blade turbines. *The American Institute of Chemical Engineers Journal*, *42*, 42–54.

Bartels, C., Breuer, M., & Durst, F. (2000). Comparison between direct numerical simulation and k–ε prediction of the flow in a vessel stirred by a Rushton turbine. *Proceedings of the 10th European conference on mixing*, (pp. 239–243).

Bertolaccini, E. (1998). *Aeration phenomena in gas–liquid stirred tank reactors*. MS thesis, University of Pisa (in italian).

Brucato, A., Ciofalo, M., Grisafi, F., & Micale, G. (1998). Numerical prediction of flow fields in baffled stirred vessel: A comparison of alternative modelling approaches. *Chemical Engineering Science*, *53*, 3654–3684.

Ciofalo, M., Brucato, A., Grisafi, F., & Torraca, N. (1996). Turbulent flow in closed and free-surface unbaffled tanks stirred by radial impellers. *Chemical Engineering Science*, *51*, 3557–3573.

De Angelis, V. (1998). *Numerical investigation and modeling of mass transfer processes at sheared gas-liquid interfaces*. Ph.D. dissertation, University of California at Santa Barbara.

Fort, I., Vonzy, M., & Forstova, B. (1991). Distribution of turbulence characteristics in agitated systems with axial high-speed impeller and baffles. *Seventh European conference on mixing* (pp. 33–41).

Harvey, A. D., Lee, C. K., & Rogers, S. E. (1995). Steady-state modeling and experimental measurement of a baffled impeller stirred tank. *The American Institute of Chemical Engineers Journal*, *41*, 2177–2186.

Harvey, A. D., & Rogers, S. E. (1996). Steady and unsteady computation of impeller-stirred reactors. *The American Institute of Chemical Engineers Journal*, *42*, 2701–2712.

Hockey, R. M., & Nouri, J. M. (1996). Turbulent flow in a baffled vessel stirred by a 60° pitched blade impeller. *Chemical Engineering Science*, *51*, 4405–4421.

Issa, R., & Ubbink, O. (1999). Numerical prediction of Taylor bubble dynamics using a new interface capturing technique. *ASME Paper FEDSM99-7103*, *Proceedings of the third joint fluids engineering conference*, July 18–23, San Francisco, California.

Jaworski, Z., Nienow, A. W., Koutsakos, E., Dyster, K., & Bujalski, W. (1991). An LDA study of turbulent flow in a baffled vessel agitated by a pitched blade turbine. *Transactions of the Institution of Chemical Engineer*, *69*, 313–320.

Jeong, J. H., & Yang, D. J. (1998). Finite element analysis of transient fluid flow with free surface using VOF (volume-of-fluid) method and adaptive grid. *International Journal for Numerical Methods in Fluids*, *26*, 1127–1154.

Kresta, S. M., & Wood, P. E. (1993a). The mean flow field produced by a 45° pitched blade turbine: Changes in the circulation pattern due to off bottom clearance. *Canadian Journal of Chemical Engineering*, *71*, 42–53.

Kresta, S. M., & Wood, P. E. (1993b). The flow field produced by a pitched blade turbine: Characterization of the turbulence and estimation of the dissipation rate. *Chemical Engineering Science*, *48*, 1761–1774.

Nagata, S. (1975). *Mixing: Principles and applications*. Tokyo, Japan: Kodansha.

Ranade, V. V., & Joshi, J. B. (1989). Flow generated by pitched blade turbines, I: Measurements using laser doppler anemometer. *Chemical Engineering Communications*, *81*, 197–224.

Ranade, V. V., Bourne, J. R., & Joshi, J. B. (1991). Fluid mechanics and blending in agitated tanks. *Chemical Engineering Science*, *48*, 1883–1893.

Ranade, V. V., Joshi, J. B., & Marathe, A. G. (1989). Flow generated by pitched blade turbines, II: Simulation using k–ε model. *Chemical Engineering Communications*, *81*, 225–248.

Sahu, A. K., & Joshi, J. B. (1995). Simulation of flow in stirred vessel with axial flow impellers: Effects of various numerical schemes and turbulence model parameters. *Industrial Engineering Chemical Research*, *34*, 626–639.

Sahu, A. K., Kumar, P., & Joshi, J. B. (1998). Simulation of flow in stirred vessel with axial flow impellers: Zonal modelling and optimization of parameters. *Industrial Engineering Chemical Research*, *37*, 2116–2130.

Sahu, A. K., Kumar, P., Patwardhan, A. W., & Joshi, J. B. (1999). CFD modelling and mixing in stirred tanks. *Chemical Engineering Science*, *54*, 2285–2293.

Scardovelli, R., & Zaleski, S. (1999). Direct numerical simulation of free-surface and interfacial flow. *Annual Review of Fluid Mechanics*, *31*, 567–603.

Schafer, M., Yianneskis, M., Wachter, P., & Durst, F. (1998). Trailing vortices around a 45° pitched blade impeller. *The American Institute of Chemical Engineers Journal*, *44*, 1233–1246.

Tatterson, G. B., Brodkey, R. S., & Calabrese, R. V. (1991). Move mixing technology into the 21st century. *Chemical Engineering Progress*, *6*, 45–48.

Tatterson, G. B., Yuan, H. S., & Brodkey, R. S. (1980). Stereoscopic visualization of the flows for pitched blade turbines. *Chemical Engineering Science*, *35*, 1369–1375.

Wechsler, K., Breuer, M., & Durst, F. (1999). Steady and unsteady computations of turbulent flow induced by a 4/45° pitched-blade impeller. *Journal of Fluid Engineering*, *ASME Transactions*, 121.

Zhou, G., & Kresta, S. M. (1996). Impact of tank geometry on the maximum turbulence energy dissipation rate for impellers. *The American Institute of Chemical Engineers Journal*, *42*, 2476–2490.